Catalysis Today 158 (2010) 348–353

Contents lists available at ScienceDirect

Catalysis Today

journal homepage: www.elsevier.com/locate/cattod

Catalytic performance of La–Ce–O mixed oxide for combustion of methane

Bo Zhang, Dao Li, Xingyi Wang*

Laboratory for Advanced Materials, Research Institute of Industrial Catalysis, East China University of Science and Technology, Shanghai 200237, China

ARTICLE INFO

Article history:
Available online 15 May 2010

Keywords:
Catalytic combustion
Methane
Ceria
Lanthanum
Solid solution

ABSTRACT

A series of Ce–La–O mixed oxide catalysts with different compositions have been prepared by sol–gel method and characterized by XRD, BET, Raman, TPR and CO_2-TPD techniques. The activity of Ce–La–O catalysts for methane oxidation has been investigated. When the ratio of Ce/Ce + La is changed from 1.0 to 0.2, only cubic phase CeO_2 with fluorite structure is observed, whose crystal size decreases significantly with the increase in La amount, due to the formation of $LaCeO_x$ solid solution. The peak at 533 °C on TPR profiles of Ce–La–O with fluorite structure is ascribed to the reduction of non-stoichiometric CeO_{2-x}. Raman bands around 570 and 1167 cm^{-1} for samples with the Ce/Ce + La ratios of 1–0.2 might be assigned to oxygen vacancies and surface superoxide ions, respectively. The addition of La promotes the formation of non-stoichiometric CeO_{2-x}, which is responsible for the oxygen vacancies and surface superoxide ions. However, when the ratio of Ce/Ce + La decreases to 0.2, ceria-in-lanthanum solid solutions are formed, where non-stoichiometric CeO_{2-x} cannot be observed. The high activity of Ce–La–O mixed oxide catalyst for methane combustion is related to superoxide ions and surface reducibility.

1. Introduction

Catalytic combustion of methane is significantly important for power generation and environment protection. The catalysts being mostly studied for this process are Pd or Pt supported catalysts, which are very expensive and prone to deactivation at high temperatures [1,2]. A variety of transition metal oxides and mixed metal oxides are another kind of catalysts showing good catalytic performance in methane combustion. However, their low surface areas lead to less activity per unit mass catalyst [3].

The fluorite structure oxides, such as ceria, zirconia, and thoria have face-centered-cubic (FCC) crystal structure in which each tetravalent metal ion is surrounded by eight equivalent nearest O^{2-} ions forming the vertices of a cube. Oxygen vacancies are created when a fluorite oxide is doped by divalent or trivalent impurity ions. Thus, the fluorite oxides have been extensively studied as oxygen ion-conducing materials, due to their high oxygen vacancy concentration and mobility properties. In the catalysis field, fluorite oxides have been explored recently as catalysts for the oxidation of carbon monoxide and methane. CeO_2-containing fluorite oxide materials are under intense scrutiny in recent years [4]. Cerium oxide, associated with other metal oxides, is shown to promote oxygen storage and release, enhance oxygen mobility, form surface and bulk oxygen vacancies, and improve the redox properties of catalysts for the oxidation process [5–7]. Therefore, it provides an opportunity to develop a new efficient catalyst system for low temperature catalytic combustion of hydrocarbons. CeO_2–La_2O_3, CeO_2–Pr_2O_3, CeO_2–ZrO_2, CeO_2–MnOx and CeO_2–CuO were used as catalysts of the oxidation of carbon monoxide, methane, soot and NO_x, and presented high activity [8–14].

The doping of La into CeO_2 could decrease the particle size, inhibit the sintering and increase the reducibility of CeO_2 [15]. Bueno-López et al. [16] proved that La^{3+} inserted into the lattice of fluorite structure to form the solid solution, and the reduction temperature of CeO_2 decreased and the catalytic performance for soot combustion was improved. Belliere et al. [17] revealed that the La enrichment at the surface of cerium–lanthanum solid solutions was an averaged effect and that the occurrence of segregation in a mixed oxide phase was observed by using electron energy-loss spectroscopy in combination with scanning transmission electron microscopy. This segregation did occur within a crystalline particle, where the dopant-rich phase was located at the surface of the dopant-deficient phase. Wilkes et al. [12–14] studied the kinetics of catalytic oxidation of CO and CH_4 on $Ce_{1-x}La_xO_{2-x/2}$ solid solution. Generally, Ce–La-based compounds exhibited good catalytic performance due to both the large oxygen storage capacity and the basicity of the surface [18]. It is believed that the rate-determined step of methane combustion is adsorption of reactant molecules on surface basic sites [19].

However, only a few studies focused on correlating the catalytic activities towards the oxidation of methane with the factors

* Corresponding author. Tel.: +86 21 64253372; fax: +86 21 64253372.
E-mail addresses: wangxy@ecust.edu.cn, wangxy1958@yahoo.com.cn (X. Wang).

0920-5861/$ – see front matter © 2010 Published by Elsevier B.V.
doi:10.1016/j.cattod.2010.04.019

such as surface species, structure defects, and oxygen vacancies of Ce–La–O catalysts. In the present work, Ce–La–O catalysts, prepared by sol–gel method, were tested in catalytic combustion of methane, and the effects of La amount varying within the whole range of composition in catalysts were investigated. Additionally, the high activity of $LaCeO_x$ solid solution was discussed in terms of various factors, including smaller ceria crystal size, increased reducibility and superoxide ions.

2. Experimental

2.1. Catalysts preparation

Ce–La–O mixed oxides, La_2O_3 and CeO_2 were prepared by sol–gel method: an aqueous solution containing $La(NO_3)_3 \cdot 6H_2O$, $Ce(NO_3)_3 \cdot 6H_2O$ (SCRC, 99.0%), and citric acid (citric acid/(La + Ce) = 1.1, molar ratio) was gradually heated to 40 °C and kept at this temperature for 3 h with stirring, resulting in the formation of a viscous gel which was then dried at 110 °C for 12 h and calcined at 550 °C for 4 h in air. Ce–La–O mixed oxides with different Ce/Ce + La ratios (X) are denoted as Ce(X)–La–O in the text.

2.2. Catalytic activity evaluation

Catalytic combustion reactions were carried out at atmospheric pressure in a micro-reactor made of a quartz tube of 4 mm in inner diameter. 200 mg catalyst was packed at the bed of the reactor. The concentrations of methane and oxygen in feed flow through the reactor were set at 0.2 and 17 mol% (balance N_2), respectively, and the gas hourly space velocity (GHSV), at 13,500 h^{-1}. The reaction temperature was measured and controlled with a thermocouple located just at the hot spot of the catalyst bed. The effluent gases were analyzed on-line at a given temperature by using a gas chromatograph (GC) equipped with TCD for the quantitative analyses of methane, CO and CO_2.

2.3. Characterization

Powder X-ray diffraction (XRD) was performed on Rigaku D/Max2 550V B/PC diffractometer employing Cu Kα radiation at 40 kV and 100 mA.

Surface areas of catalysts were estimated using the N_2 adsorption isotherm at −196 °C by the BET method on Quantachrome NOVA instrument.

Raman spectra were recorded on Via Reflex Laser Raman instrument, equipped with a CCD (charge coupled device) detector. The excitation source was the 514.5 nm line of Ar ion laser. The laser power was set at 3 mW.

Temperature-programmed reduction (TPR) measurements were carried out at atmospheric pressure in a fixed-bed reactor. 100 mg catalyst (particle size, 20–40 mesh) was loaded in a U-shaped quartz micro-reactor and the catalyst was heated to 700 °C at heating rate of 8 °C/min in a flowing hydrogen mixture (30 ml/min, 6.5% H_2 in Ar). Hydrogen consumption was monitored by using a thermal conductivity detector.

CO_2 temperature-programmed desorption (CO_2-TPD) measurements were carried out at the same apparatus for TPR. Prior to adsorption experiments, 100 mg catalyst was pre-treated in a quartz U-tube in a nitrogen stream at 700 °C for 1 h and then cooled down to 100 °C. The CO_2 adsorption was lasted for 1 h at 100 °C to saturation. Then, the desorption was carried out from 100 to 740 °C at a heating rate of 10 °C/min in nitrogen stream.

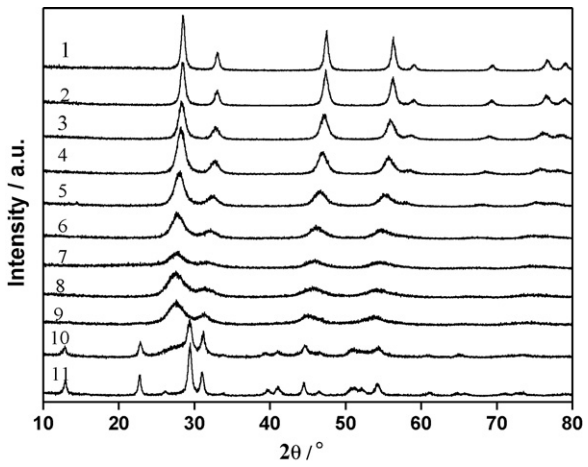

Fig. 1. XRD patterns of Ce–La–O catalysts with different ratios of Ce/Ce + La, 1-CeO_2, 2-Ce(0.80)–La–O, 3-Ce(0.75)–La–O, 4-Ce(0.70)–La–O, 5-Ce(0.60)–La–O, 6-Ce(0.50)–La–O, 7-Ce(0.40)–La–O, 8-Ce(0.30)–La–O, 9-Ce(0.20)–La–O, 10-Ce(0.10)–La–O, 11-Ce(0.05)–La–O.

3. Results and discussion

3.1. XRD characterization of Ce–La–O catalysts

Fig. 1 presents XRD patterns obtained on Ce–La–O catalysts with different ratios of Ce/Ce + La. It can be seen that the *fcc* fluorite structure of ceria, with the diffraction peaks at 2θ values of 28.6°, 33.1°, 47.5°, 56.4°, 59.1° and 69.54° [12], is retained down to the ratio of Ce/Ce + La nearly 0.2 while the *hcp* structure of lanthana is formed below the ratio of Ce/Ce + La nearly 0.1. However, the intermediate compositions between 0.1 and 0.2 form mixed phases [13]. At the upper limit of the lanthana-in-ceria solid solutions, that is, bulk composition of Ce/Ce + La ratio 0.2 [20], only CeO_2 phase with the fluorite-like structure is observed on the XRD profiles. The intensity of reflections from different crystal planes of CeO_2 phase, however, is lowered slowly with the increase in La. Moreover, the diffraction peaks of cubic fluorite structure slightly shift to higher values of the Bragg angles within the range of 28.54–27.70°, indicating that a fraction of La^{3+} can enter the fluorite lattice to form the $LaCeO_x$ solid solutions [20]. As reported in Ref. [20], the ionic radius of La^{3+} (0.106 nm) is larger than that of Ce^{4+} (0.094 nm), and the incorporation of La^{3+} into the fluorite lattice will result in the increase in the value of lattice parameter (Table 1). It also can be seen that appreciable decrease in ceria particle size parallels with an increase in La amount.

For Ce(0.05)La–O and Ce(0.10)–La–O catalysts, the reflections from the fluorite structure of CeO_2 almost disappear. There appear

Table 1
The lattice dimension and unit cell parameters of Ce–La–O catalysts.

Sample	Surface area/m^2/g	2θ (d_{111})/°	L_{111}/nm	a/Å
La_2O_3	3.8	–	–	–
Ce(0.20)–La–O	3.1	27.70	5.03	5.62
Ce(0.30)–La–O	2.7	27.60	5.00	5.58
Ce(0.40)–La–O	6.3	27.78	5.34	5.55
Ce(0.5)–La–O	25.8	27.92	6.15	5.54
Ce(0.60)–La–O	52.4	28.12	6.15	5.51
Ce(0.70)–La–O	67.0	28.24	6.97	5.47
Ce(0.75)–La–O	37.0	28.30	8.48	5.45
Ce(0.80)–La–O	32.6	28.44	11.11	5.42
CeO_2	9	28.54	13.95	5.41

Note: "L_{111}" means the size of cubic phase CeO_2 estimated according to the Scherrer equation, applied to the ⟨1 1 1⟩ reflection of the cerianite. "*a*" means the unit cell parameter, calculated by unit cell supposed that the ceria's or Ce–La–O solid solution's lattice be cubic system.

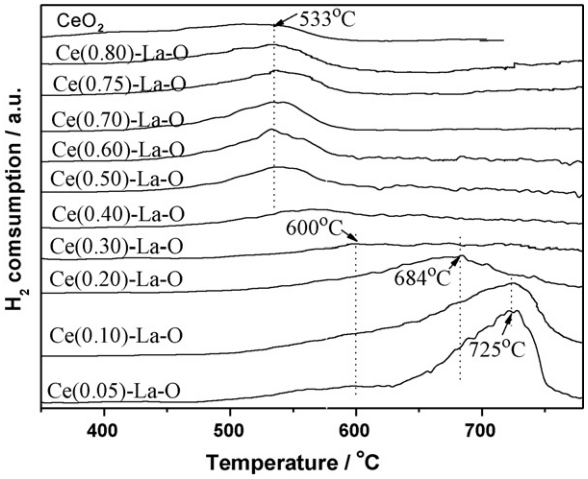

Fig. 2. TPR profiles of Ce–La–O catalysts with different ratios of Ce/Ce + La.

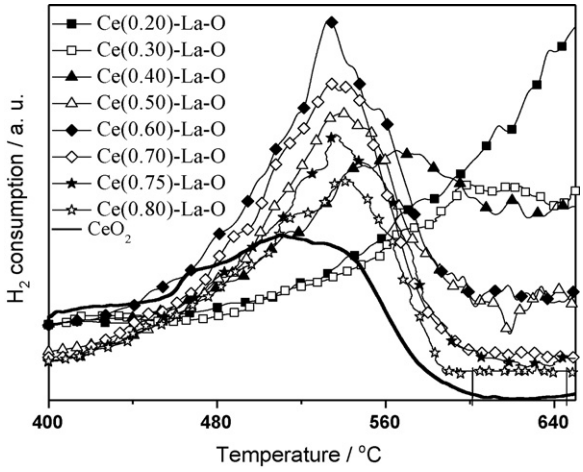

Fig. 3. The magnified part of TPR profiles of Ce–La–O catalysts with different ratios of Ce/Ce + La.

the diffraction peaks attributed to La_2O_3 (44.6°), LaOOH (29.4° and 31.1°) and $La_2O_2CO_3$ (22.3°) [21–23]. The latter two species are due to the interaction of H_2O and CO_2 in air with La_2O_3 when treated thermally. No phase related to Ce species is observed, indicating that Ce species were highly dispersed into La species structure and hence the ceria-in-lanthana solution is formed, just as the same results obtained by Wilkes et al. [12–14] and Belliere et al. [17].

Surface areas of catalysts in Table 1 were estimated by BET method based on the N_2 adsorption isotherm. La_2O_3 and CeO_2 present 3.8 and 9.0 m^2/g, respectively. For lanthana-in-ceria solid solutions, the surface areas are much larger than those of pure oxides, intermediate compositions and ceria-in-lanthana solid solutions. Here, it can be seen that the incorporation of La into CeO_2 with fluorite structure can greatly promote the dispersion of oxides. However, when the ratio of Ce/Ce + La is less than 0.6, the surface areas of catalysts decrease with the increase in La content, indicating that the dispersion of La_2O_3 decreases with the decrease of Ce.

3.2. TPR

The results of TPR analyses for Ce–La–O catalysts are shown in Fig. 2. There present three types of profiles corresponding to the samples of fluorite structure, ceria-in-lanthana solution, and intermediate structure. The reduction of pure CeO_2 occurs mainly at 533 °C within the range of experimental temperature, due to the surface oxygen removal of CeO_2. As reported [24], the peaks around 500 and 890 °C correspond to the reduction of non-stoichiometric CeO_{2-x} on the surface and bulk CeO_2, respectively. For lanthana-in-ceria solution with Ce/La + Ce ratio of greater than 0.4, the reduction peaks appear at 533 °C, which are similar to that of CeO_2, implying that the redox of Ce species on the surface of fluorite structure is not affected by the incorporation of La. However, H_2 consumption, estimated by the area under H_2-TPR profiles shown in Fig. 3, increases significantly with La content. Therefore, it can be concluded that La promotes the formation of non-stoichiometric CeO_{2-x}.

When La is increased to 60% or more, Ce^{4+} are surrounded by La^{3+} which are more electronegative, and the reduction of non-stoichiometric CeO_{2-x} shifts to higher temperature, because of "La ← O" electron-transfer processes. As a result, the peak intensity of reduction of non-stoichiometric CeO_{2-x} decreases significantly, and fluorite structure is transformed gradually into the *hcp* structure of lanthana [13] (see Fig. 1).

For ceria-in-lanthana solution in the Ce/Ce + La ratio range of 0–0.2, there appear two reduction peaks, the strong one at 684–725 °C and the weak one at 600 °C. As known, La_2O_3 can hardly be reduced under experimental condition and does not possess surface oxygen species [25]. Fleys et al. [26] suggested that the reduction of La_2O_3 at 710 °C was caused by hydroxyl group or subcarbonate species. Hoang et al. [27] attributed the similar reduction peak to the reduction of carbonaceous species on the La_2O_3 surface. In this work, the intensity of peaks at 600 and 725 °C decreases greatly for Ce(0.05)–La–O catalyst when heated at 800 °C with different time (see Fig. 4). XRD measurement shows that the diffraction peaks of $La(OH)_3$ and $La_2O_2CO_3$ cannot be observed for Ce(0.05)–La–O catalyst calcined at 800 °C. Therefore, the reduction of ceria-in-lanthana solution is related to the removal of H_2O and CO_2 from these La compounds [28]. Ce species entering La_2O_3 lattice may be reduced at higher temperature.

3.3. Raman characterization of Ce–La–O mixed oxides

Fig. 5 shows Raman spectra of Ce–La–O catalysts calcined at 550 °C. For pure CeO_2, the single sharp band around 465 cm^{-1}, ascribed to the Raman F_{2g} mode of CeO_2, as a symmetric breathing mode of the oxygen atoms surrounding each cation, is a band of fluorite structural material [29]. Since only oxygen atoms move, the

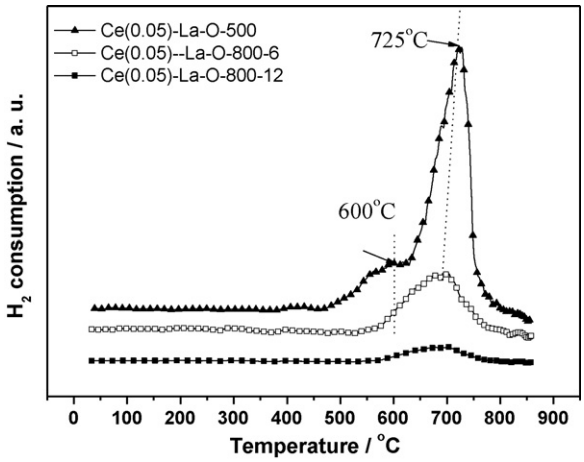

Fig. 4. TPR profiles of Ce(0.05)–La–O catalysts calcined at 800 °C with different time, Ce(0.05)–La–O-500: calcined at 500 °C, Ce(0.05)–La–O-800-6: calcined at 800 °C for 6 h, Ce(0.05)–La–O-800-12: calcined at 800 °C for 12 h.

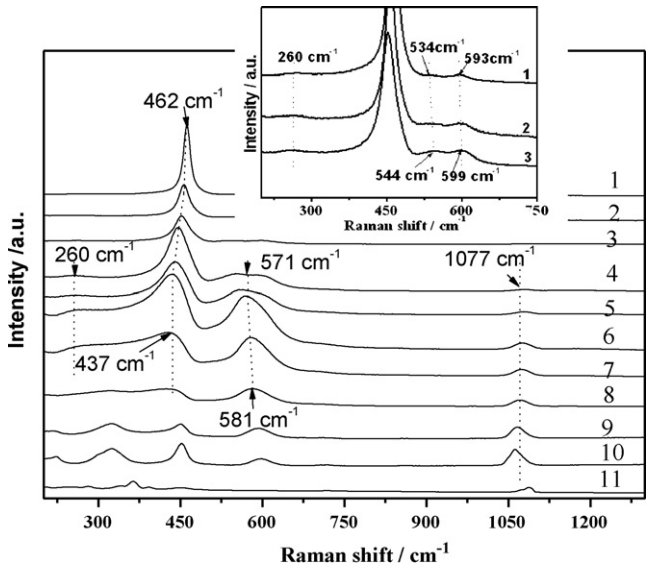

Fig. 5. Laser Raman spectra of Ce–La–O catalysts with different ratios of Ce/Ce + La, 1-Ce(0.80)–La–O, 2-Ce(0.75)–La–O, 3-Ce(0.70)–La–O, 4-Ce(0.60)–La–O, 5-Ce(0.50)–La–O, 6-Ce(0.40)–La–O, 7-Ce(0.30)–La–O, 8-Ce(0.20)–La–O, 9-Ce(0.10)–La–O, 10-Ce(0.05)–La–O, 11-La_2O_3.

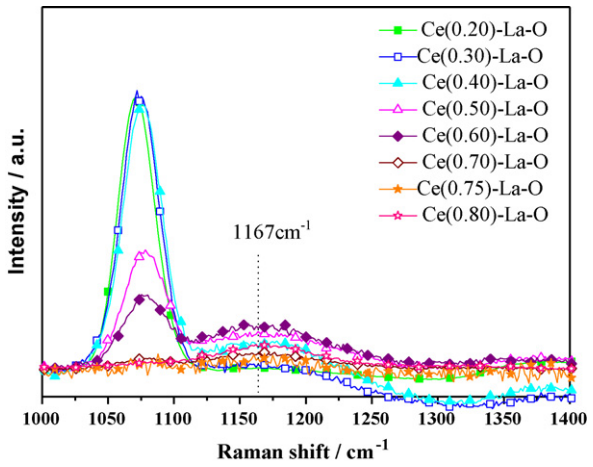

Fig. 6. The magnified part of Laser Raman spectra of Ce–La–O catalysts with different ratios of Ce/Ce + La.

mode frequency should be nearly independent of the cation mass [30]. A weak band at 1170 cm^{-1} can be due to primary A_{1g} asymmetry, combined with minor additional contributions from E_g and F_{2g} symmetries [31]. For pure lanthana, the characteristic bands of crystalline $La(OH)_3$ appear at 254, 281, 340, 449 and 598 cm^{-1} [32], and those of $La_2O_2CO_3$, at 363, 392 and 449 cm^{-1} [29]. Besides, a strong band at 1077 cm^{-1} is observed, which can be assigned to lanthanum oxycarbonate [23]. However, Raman band at 408 cm^{-1} on behalf of La_2O_3 did not appear, although the phase of La_2O_3 is observed by XRD (Fig. 1). Considering Raman as surface technology, it can be reasonable to suggest that La species on the surface combine with H_2O and CO_2 when La_2O_3 treated thermally in air to form LaOOH and $La_2O_2CO_3$, whose diffractions appear on XRD for La_2O_3 (Fig. 1).

For Ce–La–O catalysts with low content of La, such as Ce(0.80)–La–O, Ce(0.75)–La–O and Ce(0.70)–La–O, a strong band around 465 cm^{-1} ascribed to the Raman F_{2g} mode of CeO_2 [29] is observed. Moreover, with the addition of La into CeO_2, the band shifts to low wavenumbers, and its intensity becomes weaker, because the atomic mass of La is larger than that of Ce and the insertion of La ions can decrease the vibration frequency of metal–anion bond [25]. Additionally, there appear three bands, one at 260 cm^{-1} and the other two at 534–600 cm^{-1}, which will approach to each other with the increase in La, and finally combine into a strong broad band at 571 cm^{-1} when the Ce/Ce + La ratio reaches 0.3. If the ratio becomes smaller than 0.3, the band will move to higher frequency and become weaker.

McBride et al. [34] reported that in Raman spectra the F_{2g} mode of $Ce_{1-x}RE_xO_{2-y}$ solid solutions becomes asymmetric with the presence of a long low-frequency tail as the value x increases, and there is also a weak band around 570 cm^{-1} on the high frequency side of the band. However, the presence of some defects can involve relaxation of the selection rules. This band, in particular, is linked with the oxygen vacancies in the CeO_2 lattice [34]. The reason for the formation of the band at 570 cm^{-1} is that when two Ce^{4+} ions are substituted by two La^{3+} ions, one oxygen vacancy is introduced into the fluorite lattice in order to maintain the electrical neutrality, so as to cause the broad peak on the high frequency side of the F_{2g} band. Thus the band can be linked with lattice defects which result in the creation of oxygen vacancies. With the increase of La, the concentration of oxygen vacancies increases, and the action of cations on oxygen vacancies becomes weak, leading to the increase in frequency of corresponding band. Moreover, when the Ce/Ce + La ratio is 0.4, the intensity of band at 570 cm^{-1} reaches maximum, that is, the number of oxygen vacancies reaches maximum. Combined with the XRD patterns in Fig. 1, it is suggested that the oxygen vacancies in the solid solutions increase when the fluorite structure of Ce–La–O catalysts becomes more defective. This is different from the case of doping ceria with Pr^{3+} cations [9], in which the oxygen vacancies are orderly arranged in the solid solutions and the proportion of Ce and Pr can be well situated. It is noted that the changing trend of the intensity for the band at 260 cm^{-1} can be correlated with that of the band at 570 cm^{-1}, indicating that the band at 260 cm^{-1} may be due to the other asymmetric vibration caused by the formation of oxygen vacancies. Additionally, the band at 1077 cm^{-1} of $La_2O_2CO_3$ [28] becomes stronger and more symmetric with the decrease in the Ce/Ce + La ratio from 0.6 to 0.05, where no other band of La species is observed, which confirms that La species on the surface presents mainly in the form of $La_2O_2CO_3$.

Fig. 6 is a magnified part of Raman spectra in the range of 1100–1400 cm^{-1}. Long and Wan confirmed that the Raman bands at 1040 and 1172 cm^{-1} were caused by surface superoxide ions which were active for oxidation of methane [35]. Here, the weak band at 1167 cm^{-1} might be assigned to surface superoxide ions [36], which are generated due to the insertion of La^{3+} and the formation of defects. The band weakens in the order as follows: Ce(0.60)–La–O > Ce(0.70)–La–O > Ce(0.50)–La–O > Ce(0.75)–La–O > Ce(0.80)–La–O > Ce(0.40)–La–O > Ce(0.30)–La–O > Ce(0.20)–La–O, which is consistent with the intensity order of the reduction of non-stoichiometric CeO_{2-x}. For the catalysts with Ce/Ce + La ratios of greater than 0.4, the reducibility of non-stoichiometric CeO_{2-x} is influenced by "La ← O" electron-transfer processes and thus decrease with increase of La content.

The formation of oxygen vacancies is caused by the substitution of La^{3+} ions for Ce^{4+}, which results in the defects of fluorite structure. Thus, the fluoride oxides have been extensively studied as oxygen-ion-conducting materials [37]. As known, non-stoichiometric CeO_{2-x} is resulted from defective structure. It can be proposed that defects are responsible for the oxygen vacancies which can be related to non-stoichiometric CeO_{2-x}. The fact that when Ce/Ce + La is less than 0.5, the reduction of non-stoichiometric CeO_{2-x} becomes weak and shifts to high temperature (Fig. 3) indicates that the environment of oxygen vacancies is also is influenced by the "La ← O" electron-transfer processes.

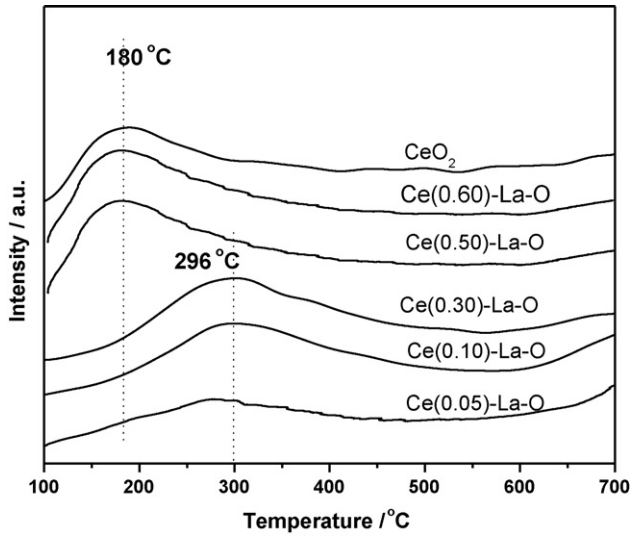

Fig. 7. CO_2-TPD profiles of Ce–La–O catalysts with different ratios of Ce/Ce + La.

3.4. CO_2-TPD

The CO_2-TPD profiles on Ca–La–O catalysts are shown in Fig. 7. For fluorite structure solution with the Ce/Ce + La ratio of greater than 0.5, CO_2 desorption with maxima at 180 °C was observed. Wilkes et al. [12] reported that CO_2 desorption occurred at 120 °C on CeO_2. Obviously, CeO_2 is responsible for the surface basicity of the samples with fluorite structure. Moreover, the base amount (area under the profiles) parallels with La content. As known, the basic strength of oxides can be controlled by modifying the number of defects in the framework of the materials [38], i.e. the number of oxygen atoms which associate with Ce with a low coordination number. The addition of La cannot modify the basic strength of catalysts with fluorite structure, indicating that the coordination of oxygen atom with Ce^{4+} on the surface is not influenced by La^{3+}, which, in turn, enters CeO_2 and causes the increase in dispersion of Ce^{4+} so as to increase the surface basicity.

For catalysts with ceria-in-lanthana solution and intermediate structure, CO_2 desorption occurs at higher temperature, 296 °C, compared with catalysts with fluorite-like structure. The stronger basicity is related to more La species existing on the surface. As known, La_2O_3, a strong solid base, can react with H_2O and CO_2 in air to form LaOOH and $La_2O_2CO_3$, respectively [12]. The surface basicity decreases significantly with the La content because of the formation of more amount of $La_2O_2CO_3$, as indicated by XRD and Raman. It is interesting to find that the basicity cannot be modified by changing the doping amount of Ce, that is, the coordination of oxygen atom with La^{3+} on the surface ceria-in-lanthana is not influenced by Ce^{4+}. Belliere et al. [17] revealed that the La enrichment at the surface of ceria-in-lanthana solid solution was an averaged effect. It can be deduced that La enrichment occurs on the surface of ceria-in-lanthana solid solution and intermediate structure. For the similar reason as above mentioned, Ce^{4+} can enter lanthana phase, and cause the increase in dispersion of La species, so that the surface basicity increases.

3.5. Oxidation activity

Fig. 8 illustrates the results of activities of the Ce–La–O mixed oxides catalysts for methane combustion. $T_{50\%}$ and $T_{90\%}$ (the temperature needed to reach 50 and 90% conversion, respectively) are shown in Fig. 9, in which the activity is observed as a function of the ratio of Ce/Ce + La. The reaction product is mainly CO_2, and no other by-product was detected. Ce(0.6)–La–O shows the

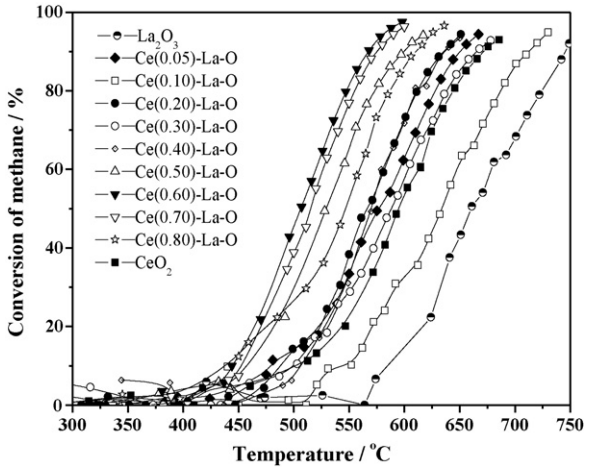

Fig. 8. The catalytic activity of over Ce–La–O catalysts with different ratios of Ce/Ce + La for CH_4 combustion, gas composition: 0.2% CH_4, 10% O_2, N_2 balance; GHSV = 13,500 h^{-1}.

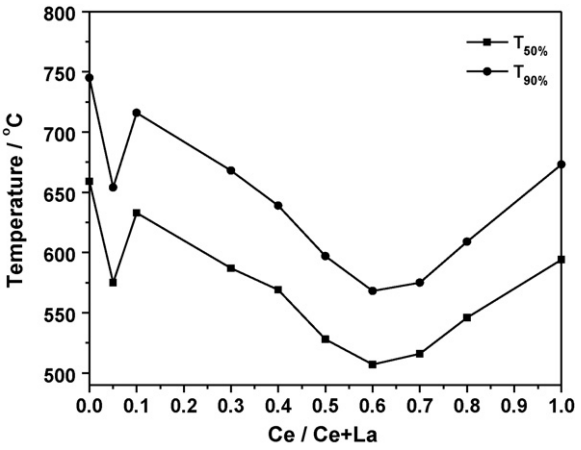

Fig. 9. $T_{50\%}$ and $T_{90\%}$ for CH_4 catalytic combustion over Ce–La–O catalysts with different ratios of Ce/Ce + La, gas composition: 0.2% CH_4, 10% O_2, N_2 balance; GHSV = 13,500 h^{-1}.

best catalytic activity, and $T_{50\%}$ and $T_{90\%}$ are 550 and 575 °C, respectively. However, with the increase in Ce/Ce + La ratio from 0.70 to 1, $T_{50\%}$ and $T_{90\%}$ shift to high temperature to some extent. Luo et al. reported that the conversion of methane reached 90% at 600 °C on Ce–Pr-0.4 catalyst, and the high methane oxidation activity can be attributed to more mobility of bulk oxygen in catalysts [29]. In this work, the order of activity is as follows: Ce(0.60)–La–O > Ce(0.70)–La–O > Ce(0.50)–La–O > Ce(0.80)–La–O > Ce(0.40)–La–O > Ce(0.30)–La–O > Ce(0.20)–La–O, which is consistent with the intensity orders of superoxide ions in Raman spectra and reduction peak of non-stoichiometric CeO_{2-x} at 530 °C in TPR. It is supposed that methane can adsorb readily onto oxygen vacancies and then can react with superoxide ions, which may be promoted by non-stoichiometric CeO_{2-x}. Additionally, the translation of gas oxygen to surface active species (superoxide ions) may be promoted by oxygen vacancies. Therefore, the high activity of Ce–La–O catalysts can be attributed to the combination of superoxide ions and surface reducibility.

The catalysts with Ce/Ce + La ratio less than 0.3 do not perform very well in the catalytic combustion of methane and present the worst activity of La_2O_3 catalyst. From XRD and Raman results of the these samples, $La_2O_2CO_2$ or $La(OH)_2$ are observed. CO_2-TPD tests show that these La species have strong basicity. According to the work by Wilkes [12] and his group, carbon dioxide strongly retards

the catalytic combustion of methane over lanthana and ceria. Liu and Flytzani-Stephanopoulos [18,19] suggested that the strength and geometry of acidic and basic sites on the catalyst surface played an important role for C–H bond breakage. Here, basic La species should be favorable for the activation of methane molecule. However, there is almost no surface active oxygen for the samples in the form of ceria-in-lanthana solution, and hence the oxidation of methane becomes difficult.

4. Conclusion

The activity for methane oxidation exhibited by a series of Ce–La–O catalysts with different compositions prepared by sol–gel method has been investigated. The incorporation of La into CeO_2 promotes the formation of non-stoichiometric CeO_{2-x}, which is responsible for oxygen vacancies and superoxide ions. As a result, the high activity of Ce–La–O catalysts with fluorite structure towards the oxidation of methane is observed.

Acknowledgements

We would like to acknowledge the financial support from National Basic Research Program of China (No. 2010CB732300), National Natural Science Foundation of China (No. 20977029) and the Commission of Science and Technology of Shanghai Municipality (0852nm00900).

References

[1] K. Sekizawa, H. Widjaja, S. Maeda, Catal. Today 59 (2000) 69.
[2] W. Lin, L. Lin, Y.X. Zhu, Y.C. Xie, K. Scheurell, E. Kemnitz, Appl. Catal. B: Environ. 57 (2005) 175.
[3] A.F. Lucrédio, G. Jerkiewicz, E.M. Assaf, Appl. Catal. B: Environ. 84 (2008) 106.
[4] S.F. Zuo, Q.Q. Huang, J. Li, R.X. Zhou, Appl. Catal. B: Environ. 91 (2009) 204.
[5] V. Ramaswamy, S. Malwadkar, S. Chilukuri, Appl. Catal. B: Environ. 84 (2008) 21.
[6] L.F. Liotta, G. Di Carlo, G. Pantaleo, G. Deganello, Catal. Commun. 6 (2005) 329.
[7] L.F. Liotta, G. Di Carlo, G. Pantaleo, A.M. Venezia, G. Deganello, Appl. Catal. B: Environ. 66 (2006) 217.
[8] I. Atribak, A. Bueno-López, A. García-García, J. Catal. 259 (2008) 123.
[9] M. Kramer, W.F. Maier, Appl. Catal. A: Gen. 302 (2006) 257.
[10] J. Liu, Z. Zhao, J. Wang, C.M. Xu, A.J. Duan, Appl. Catal. B: Environ. 84 (2008) 185.
[11] P. Djinovic, J. Batista, A. Pintar, Appl. Catal. A: Gen. 347 (2008) 23.
[12] M.F. Wilkes, P. Hayden, A.K. Bhattacharya, J. Catal. 219 (2003) 286.
[13] M.F. Wilkes, P. Hayden, A.K. Bhattacharya, J. Catal. 219 (2003) 295.
[14] M.F. Wilkes, P. Hayden, A.K. Bhattacharya, J. Catal. 219 (2003) 305.
[15] L. Kundakovic, M. Flytzani-Stephanopoulos, J. Catal. 179 (1998) 203.
[16] A. Bueno-López, K. Krishna, M. Makkee, J.A. Moulijn, J. Catal. 230 (2005) 237.
[17] V. Belliere, G. Joorst, O. Stephan, F.M.F. de Groot, B.M. Weckhuysen, J. Phys. Chem. B 110 (2006) 9984.
[18] W. Liu, M. Flytzani-stephanopoulos, J. Catal. 153 (1995) 304.
[19] W. Liu, M. Flytzani-stephanopoulos, J. Catal. 153 (1995) 317.
[20] M.F. Wilkes, P. Hayden, A.K. Bhattacharya, Appl. Surf. Sci. 206 (2003) 12.
[21] T.H. Fleisch, R.F. Hicks, A.T. Bell, J. Catal. 87 (1984) 398.
[22] S. Bernal, F.J. Botana, R. Garcia, F. Ramirez, Appl. Catal. 31 (1987) 267.
[23] B. Klingenberg, M.A. Vannice, Chem. Mater. 8 (1996) 2755.
[24] H.C. Yao, Y.F. Yu Yao, J. Catal. 86 (1984) 254.
[25] G. Groppi, C. Cristiani, L. Lietti, C. Ramella, M. Valentini, P. Forzatti, Catalysis 50 (1999) 399.
[26] M. Fleys, Y. Simon, D. Swierczynski, A. Kiennemann, P.M. Marquaire, Energy Fuel 20 (2003) 2321.
[27] D.L. Hoang, A. Dittmar, J. Radnik, K.W. Brzezinka, K. Witke, Appl. Catal. A: Gen. 239 (2003) 95.
[28] E.S. Putna, B. Shereck, R.J. Gorte, Appl. Catal. B: Environ. 17 (1998) 101.
[29] M.F. Luo, Z.L. Yan, L.Y. Jin, J. Mol. Catal. A: Chem. 260 (2006) 157.
[30] V.G. Keramidas, W.B. White, J. Chem. Phys. 59 (1973) 1561.
[31] W.H. Weber, K.C. Hass, J.R. McBride, Phys. Rev. B 48 (1993) 178.
[32] G. Gallaher, J. Goodwin, C. Huang, M. Houalla, J. Catal. 140 (1993) 453.
[34] J.R. McBride, K.C. Hass, B.D. Poindexter, W.H. Weber, J. Appl. Phys. 76 (1994) 2435.
[35] R.Q. Long, H.L. Wan, J. Chem. Soc., Faraday Trans. 93 (1997) 355.
[36] C. Binet, M. Daturi, J.-C. Lavalley, Catal. Today 50 (1999) 207.
[37] H.L. Tuller, D.K. Moon, Sci. Engl. B1 171 (1988) 1.
[38] C. Chizallet, G. Costentin, H. Lauron-Pernot, J.M. Krafft, P. Bazin, J. Saussey, F. Delbecq, P. Sautet, M. Che, Oil Gas Sci. Technol. 61 (2006) 479.